Coarse-grained model of conformation-dependent electrophoretic mobility and its influence on DNA dynamics

Harsh Pandey and Patrick T. Underhill[*]

The Howard P. Isermann Department of Chemical and Biological Engineering, Rensselaer Polytechnic Institute, Troy, New York 12180, USA

The electrophoretic mobility of molecules such as λ-DNA depends on the conformation of the molecule. It has been shown that electrohydrodynamic interactions between parts of the molecule lead to a mobility that depends on conformation and can explain some experimental observations. We have developed a new coarse-grained model that incorporates these changes of mobility into a bead-spring chain model. Brownian dynamics simulations have been performed using this model. The model reproduces the cross-stream migration that occurs in capillary electrophoresis when pressure-driven flow is applied parallel or antiparallel to the electric field. The model also reproduces the change of mobility when the molecule is stretched significantly in an extensional field. We find that the conformation-dependent mobility can lead to a new type of unraveling of the molecule in strong fields. This occurs when different parts of the molecule have different mobilities and the electric field is large.

PACS number(s): 82.45.−h, 83.10.Mj, 83.80.Rs, 82.35.Rs

I. INTRODUCTION

Electrophoresis of molecules such as DNA often occurs in situations in which the conformation of the molecule is disturbed from its equilibrium coiled state. This occurs in gel electrophoresis, in electric field gradients, and when fluid flows are simultaneously applied to the molecules [1–4]. When the coil is disturbed, it is important to include the electrohydrodynamic interactions between segments [5]. For example, it has been shown that these interactions lead to migration of molecules across field lines and changes of mobility with conformation [6–10].

There have been two main approaches to incorporate the electrohydrodynamic interactions into theoretical and/or simulation models of electrophoresis. Butler, Ladd, and co-workers [9] developed a simulation method that includes directly the interactions between segments of a bead-spring chain polymer model. Lee, Larson, and co-workers [11] developed a model that ignores the long ranged electrohydrodynamic interactions but includes the local electrohydrodynamic interactions within a Kuhn segment along the polymer backbone. The first approach has been used successfully when the polymer is weakly deformed from equilibrium. If the method is to work accurately for large deviations from equilibrium, a large number of springs would need to be included in the model, increasing the computational cost. The second approach has been used to qualitatively understand the changes of mobility with conformation when molecules are strongly stretched in field gradients. However, the approach assumes that the polymer is stretched along the field direction and is therefore not able to capture migration across field lines.

In this article, we develop and validate a coarse-grained computational model that incorporates the change of the polymer mobility with conformation in an efficient way that can be used for molecules both near and far from the equilibrium coiled state. Using this model, we show that the stretching of molecules in strong extensional gradients can

occur differently than is typically seen in simulations and experiments.

II. MODEL DEVELOPMENT

A. Hydrodynamic versus electrohydrodynamic interactions

In the dynamics of dilute uncharged polymer solutions, it is important to include hydrodynamic interactions in order to capture many dynamical quantities such as drag on the polymer, diffusivity, and relaxation time spectrum [12]. This is the case both when the polymer is in an equilibrium coiled state and when the polymer is in a highly stretched state. One way to see this mathematically, which has been used previously in the literature [13], is to consider a typical polymer segment and calculate the net flow produced by the other polymer segments. The average velocity on a typical polymer segment is an integral of the disturbance caused by the other polymer segments. Mathematically, this is written as

$$\boldsymbol{v}_{\text{ave}} = \int \boldsymbol{G} \cdot \boldsymbol{F} \rho \, dV, \tag{1}$$

where ρ is the density of other polymer segments in a region of volume dV, $\boldsymbol{F}$ is the force on the fluid by those polymer segments, and $\boldsymbol{G}$ is the Green's function that is used to calculate the flow generated in the fluid by that force. In order to understand the generic differences between hydrodynamic interactions (HIs) and electrohydrodynamic interactions (EHIs), we make approximations to investigate the scaling of the integral. For example, we examine the case in which $\boldsymbol{F}$ is a constant and so can be removed from the integral. We also assume that ρ is approximately constant within the region that the polymer segments occupy. The key difference between HI and EHI is the dependence of $\boldsymbol{G}$ on angle and the scaling with r, the separation of two polymer segments. The Green's function for HI is the Oseen tensor, which is given by

$$\boldsymbol{G}_{HI} \propto \frac{1}{r}(\hat{\boldsymbol{r}}\hat{\boldsymbol{r}} + \boldsymbol{I}), \tag{2}$$

where $\hat{\boldsymbol{r}}$ is a unit vector pointing in the radial direction and $\boldsymbol{I}$ is the identity tensor. The key features are that it scales as r^{-1} and has a nonzero average over angle. However, the Green's

————
[*]Corresponding author: underhill@rpi.edu

function for EHI is

$$\boldsymbol{G}_{EHI} \propto \frac{1}{r^3}(3\hat{r}\hat{r} - \boldsymbol{I}), \tag{3}$$

which scales as r^{-3} and has a zero average over angle.

Using these approximations and the characteristics of the Green's functions, the average velocity in the equilibrium coiled state for the HI and EHI cases are

$$\boldsymbol{v}_{\mathrm{ave},HI,eq} \sim \boldsymbol{F}(\text{angular average}) \int_{\ell}^{R} \frac{1}{r} r^2 dr, \tag{4}$$

$$\boldsymbol{v}_{\mathrm{ave},EHI,eq} \sim \boldsymbol{F}(\text{angular average}) \int_{\ell}^{R} \frac{1}{r^3} r^2 dr, \tag{5}$$

where the lower limit of integration ℓ represents the radius at which the far field Green's function is no longer valid and R is the radius of the polymer coil. In the HI case, the angular average is finite, and the radial integral has a dependence on R. This dependence on the polymer coil size shows that long range HI between polymer segments within the coil are important. In the EHI case, the radial integral also has R dependence, but the angular integral vanishes. Therefore, exactly at equilibrium, the EHI contributions do not affect the net drag on the polymer coil, which leads to a mobility that is independent of length in free solution electrophoresis.

When the polymer is strongly stretched (e.g., along the direction of $\boldsymbol{F}$), the integral over polymer segments becomes an integral along a line instead of throughout a sphere. The average velocities in this stretched state then become

$$\boldsymbol{v}_{\mathrm{ave},HI,st} \sim \boldsymbol{F} \int_{\ell}^{L} \frac{1}{r} dr, \tag{6}$$

$$\boldsymbol{v}_{\mathrm{ave},EHI,st} \sim \boldsymbol{F} \int_{\ell}^{L} \frac{1}{r^3} dr, \tag{7}$$

where L is the contour length of the stretched polymer. The HI case again depends on the size of the polymer (the contour length in this case). However, for large L, the EHI case no longer depends on L.

This scaling analysis shows that long ranged HIs are important to include both near equilibrium and in an extended conformation. For EHIs, they cancel right at equilibrium and long ranged interactions can be ignored for long polymers in extended conformations. The simulation approach of Butler, Ladd, and co-workers [9] was to include directly the long ranged EHI in systems weakly perturbed from equilibrium. They showed that when the angular symmetry is broken, the EHI is important and leads to migration across field lines. One disadvantage of the model is that if the polymer is stretched, the long ranged interactions play a very small role. In order to include the role of short ranged interactions, a large number of beads would need to be included, increasing the computational cost. In contrast, the work of Lee, Larson, and co-workers [11] examined highly stretched chains and therefore ignored long ranged interactions. Instead, they included the interactions between two polymer segments within a single rod (Kuhn length). As the polymer is stretched, the rods are oriented, which leads to a change in the mobility. However, they did not incorporate this change into a mobility that can be used

in dynamical simulations. In this work, we use the approach of Lee and Larson to develop a mobility tensor, then use that mobility tensor in dynamical simulations. This approach is similar to Brownian dynamics simulations in which the drag coefficient on a bead varies with the stretch of the polymer (due to HIs), though this drag coefficient is typically taken as a scalar instead of a tensor [14–16].

B. Conformation-dependent mobility

Our modeling approach is to consider the polymer to be a freely jointed chain (FJC) which is coarse-grained to a bead-spring chain model. Although double-stranded DNA (ds-DNA) in highly extended configurations is more accurately represented as a wormlike chain, the FJC slightly simplifies the analysis while retaining the key qualitative features. Each spring represents the free energy of the chain averaged over the configurations of the rods of the polymer that the spring represents. We also assign to that spring an electrophoretic mobility tensor which is derived by considering the mobilities of the underlying rods. Following the approach of Lee and Larson [11], consider a rod which represents a Kuhn length in the FJC model with unit vector $\boldsymbol{u}$ along its axis. This rod has an electrophoretic mobility tensor $\boldsymbol{M}$, which can be written as

$$\boldsymbol{M} = M_{\parallel}\boldsymbol{u}\boldsymbol{u} + M_{\perp}(\boldsymbol{I} - \boldsymbol{u}\boldsymbol{u}), \tag{8}$$

where $\boldsymbol{I}$ is the identity tensor. If we only had a single rod in an electric field, this mobility would determine the velocity of the rod for which the electric field and flow drag forces balance. In a polymer, the rods are connected together so that the rods do not move at this velocity. Their actual velocity also depends on their hydrodynamic drag coefficient tensor $\boldsymbol{Z}$ given by

$$\boldsymbol{Z} = \zeta_{\parallel}\boldsymbol{u}\boldsymbol{u} + \zeta_{\perp}(\boldsymbol{I} - \boldsymbol{u}\boldsymbol{u}). \tag{9}$$

Using the notation in Ref. [11], we can write $M_{\parallel} = \mu_0 + 2\mu_1$ and $M_{\perp} = \mu_0 - \mu_1$, where μ_0 and μ_1 are functions of the charge density, Debye length, Kuhn length, solvent viscosity, etc. If the mobility of the rod were isotropic, then $\mu_1 = 0$. If the Kuhn length is longer than it is wide, and the Debye length is larger than the width but smaller than the Kuhn length, then $\mu_1 \approx \mu_0/4$. Note that we are assuming that the Debye length is small enough that the ion clouds are not disturbed by the electric field or fluid flow. In the notation used here, the effective mobility of the FJC is denoted by $\boldsymbol{\mu}$ and was shown by Ref. [11] to solve

$$\langle \boldsymbol{Z} \rangle \cdot \boldsymbol{\mu} = \langle \boldsymbol{Z} \cdot \boldsymbol{M} \rangle, \tag{10}$$

where the angle brackets denote an average over the orientation distribution of the rods. This distribution is not isotropic and is restricted by the extension of the chain; if the chain is near equilibrium, the rods will be almost isotropic while if the chain is stretched the rods will be highly aligned. The approach in our model is to approximately determine this distribution from the extension of a spring in the coarse-grained model, calculate the averages over $\boldsymbol{u}$ to determine the effective mobility of the spring $\boldsymbol{\mu}$, then use that mobility in the dynamics of the spring.

Consider a spring whose extension vector is denoted as $\boldsymbol{Q}$ and whose maximum extension is $Q_0 = N_k A_k$, where N_k is the number of Kuhn steps that the spring represents and A_k is the Kuhn length. The spring with extension $\boldsymbol{Q}$ represents an average over all FJC configurations for which the end to end

vector is Q. Therefore, the extension must be related to the average of a rod $Q = N_k A_k \langle u \rangle$. To simplify the notation, we denote $n \equiv \langle u \rangle$, so that $Q/Q_0 = n$. In this way, the stretch of the spring determines the average of the rod orientation vector, but does not directly determine the distribution. We follow a similar approach as Lee and Larson and postulate that the distribution is the one in which the rod is subject to an external "force" f and the force is determined such that the average over the distribution is the correct known average. Therefore, the probability distribution of rod angles is $P(u) \propto \exp[\beta f(n) \cdot u]$, where $\beta = 1/(k_B T)$ and we have explicitly noted that the force is a function of the average u.

This choice is only self-consistent if we calculate the average angle and obtain n. Because of the form of this distribution, we can calculate the average analytically. This self-consistency requires that we choose the force as

$$f(n) = \frac{\mathcal{L}^{-1}(n)}{\beta} \frac{n}{n}, \tag{11}$$

where the nonboldface n denotes the magnitude of the vector and $\mathcal{L}^{-1}$ is the inverse Langevin function $[\mathcal{L}(x) = \coth x - 1/x]$. Plugging Eqs. (9) and (8) into (10) and using that u is a unit vector gives the key equation we must solve for the effective mobility μ,

$$[(\zeta_\parallel - \zeta_\perp)\langle uu \rangle + \zeta_\perp I] \cdot \mu = (\zeta_\parallel M_\parallel - \zeta_\perp M_\perp)\langle uu \rangle$$
$$+ \zeta_\perp M_\perp I. \tag{12}$$

We must now use the Boltzmann distribution to perform the average of the second moment of the vector u. This can also be calculated analytically to be

$$\langle uu \rangle = \left(1 - \frac{3n}{\beta f}\right)\hat{n}\hat{n} + \frac{n}{\beta f}I, \tag{13}$$

where the hat over the vector means the unit vector in the direction of the vector. We can see that the effective mobility will be of the form

$$\mu = \mu_\parallel \hat{n}\hat{n} + \mu_\perp (I - \hat{n}\hat{n}). \tag{14}$$

Plugging this and Eq. (13) into Eq. (12), we can solve for the effective mobility parallel and perpendicular to the spring

$$\mu_\parallel = \frac{(\zeta_\parallel M_\parallel - \zeta_\perp M_\perp)\left(1 - \frac{2n}{\beta f}\right) + \zeta_\perp M_\perp}{(\zeta_\parallel - \zeta_\perp)\left(1 - \frac{2n}{\beta f}\right) + \zeta_\perp}, \tag{15}$$

$$\mu_\perp = \frac{(\zeta_\parallel M_\parallel - \zeta_\perp M_\perp)\frac{n}{\beta f} + \zeta_\perp M_\perp}{(\zeta_\parallel - \zeta_\perp)\frac{n}{\beta f} + \zeta_\perp}. \tag{16}$$

In summary, these two equations give the effective mobility of a spring which represents a FJC where the ζ and M are the drag coefficients and mobilities of a rod of the FJC. Since $Q/Q_0 = n$, n is the fractional extension of the spring, $\hat{n}$ is a unit vector directed along the spring, and f is given by the self-consistency condition in Eq. (11). It is useful to point out some important limiting cases of Eqs. (15) and (16). This will provide physical insight into the nature of the formulas.

The first special case is $M_\parallel = M_\perp$. In this limit, the rod has an isotropic mobility, and the formulas lead to an isotropic mobility for the spring $\mu_\parallel = \mu_\perp$. The second special case is $\zeta_\parallel = \zeta_\perp$. In this limit, the drag coefficient is isotropic,

and the formulas lead to a spring mobility which is a linear combination of the rod mobilities. If the drag coefficient is not isotropic, the spring mobility is still a linear combination of the rod mobilities but the drag coefficients change how strongly the rod mobilities are weighted.

The one complication using these effective mobilities in a bead-spring chain simulation is the inverse Langevin function in Eq. (11). Computing this inverse for each spring at each time step would make the method more computationally costly. A Padé approximant has been previously developed by Cohen to approximate the inverse Langevin function [17]. This approximation is $\beta f = \mathcal{L}^{-1}(n) \approx (3n - n^3)/(1 - n^2)$. With this approximation, the spring mobilities become an explicit function of n, the fractional extension of the spring, as

$$\mu_\parallel = \frac{(\zeta_\parallel M_\parallel - \zeta_\perp M_\perp)\left(\frac{1+n^2}{3-n^2}\right) + \zeta_\perp M_\perp}{(\zeta_\parallel - \zeta_\perp)\left(\frac{1+n^2}{3-n^2}\right) + \zeta_\perp}, \tag{17}$$

$$\mu_\perp = \frac{(\zeta_\parallel M_\parallel - \zeta_\perp M_\perp)\left(\frac{1-n^2}{3-n^2}\right) + \zeta_\perp M_\perp}{(\zeta_\parallel - \zeta_\perp)\left(\frac{1-n^2}{3-n^2}\right) + \zeta_\perp}. \tag{18}$$

In the case of $\zeta_\parallel = \zeta_\perp$, these simplify, respectively, to

$$\mu_\parallel = (M_\parallel - M_\perp)\left(\frac{1+n^2}{3-n^2}\right) + M_\perp, \tag{19}$$

$$\mu_\perp = (M_\parallel - M_\perp)\left(\frac{1-n^2}{3-n^2}\right) + M_\perp. \tag{20}$$

If we use the definitions $M_\parallel = \mu_0 + 2\mu_1$ and $M_\perp = \mu_0 - \mu_1$, the mobilities become, respectively,

$$\mu_\parallel = \mu_0 + \frac{4\mu_1 n^2}{3 - n^2}, \tag{21}$$

$$\mu_\perp = \mu_0 - \frac{2\mu_1 n^2}{3 - n^2}. \tag{22}$$

C. Simulation methodology

In this work we use the standard Brownian dynamics simulation methodology [18–22]. The polymer is modeled as a bead-spring chain, in which the solvent and dissolved ions are treated as a continuum that gives rise to viscous drag, Brownian fluctuations, and HIs. In the bead-spring chain model, the bead positions are tracked and they are the points where the hydrodynamic and electric field forces are applied. The stochastic equation for the change in the position of bead i is

$$dr_i = \left[u^\infty(r_i) + \sum_{j=1}^{N_b} P_{ij} \cdot E(r_j) + \frac{1}{k_B T} \sum_{j=1}^{N_b} H_{ij} \cdot F_j \right.$$
$$\left. + \sum_{j=1}^{N_b} \frac{\partial}{\partial r_j} \cdot H_{ji} \right] dt + \sqrt{2dt} \sum_{j=1}^{N_b} B_{ij} \cdot dW_j, \tag{23}$$

where N_b is the number of beads, r_i is the position of bead i, u^∞ is the imposed external fluid flow evaluated at the position of the bead, P_{ij} is the effective electrophoretic mobility tensor describing how fields at bead j alter the motion of bead i, E is the external electric field evaluated at the position of bead j, H_{ij} is the hydrodynamic diffusion tensor, F_j is the net of

spring forces and excluded volume forces on bead j, and $d\boldsymbol{W}_j$ is a vector of random variables with zero mean and variance 1. In order to satisfy the fluctuation-dissipation theorem, the tensor $\boldsymbol{B}_{ij}$ must obey

$$\boldsymbol{H}_{ij} = \sum_{k=1}^{N_b} \boldsymbol{B}_{ik} \cdot \boldsymbol{B}_{jk}^T. \tag{24}$$

Throughout most of the article we will utilize our new model which only includes EHIs within a rod of the FJC and not between rods. These mean that the mobility tensor $\boldsymbol{P}_{ij}$ is zero if $i \neq j$ and equals $\boldsymbol{\mu}_i$ when $i = j$. The mobility of a spring is determined as a function of the stretch of the spring using Eqs. (21) and (22). In particular, the mobility tensor is

$$\boldsymbol{\mu} = \left(\mu_0 + \frac{4\mu_1 n^2}{3 - n^2}\right)\hat{\boldsymbol{n}}\hat{\boldsymbol{n}} + \left(\mu_0 - \frac{2\mu_1 n^2}{3 - n^2}\right)(\boldsymbol{I} - \hat{\boldsymbol{n}}\hat{\boldsymbol{n}}). \tag{25}$$

If a bead is connected to two springs, the mobility used for the bead is the average of the mobilities of the springs. In this article, we do not consider HIs between polymer segments or between the polymer segments and the channel walls. For polymers that are relatively short, as considered here, HI between polymer segments only have a small impact on the nature of polymer stretching. Additionally, it has been shown that for the conditions examined here, the migration of polymers due to wall-mediated HI is small if the Weissenberg number is not too large [9]. We have verified this in our simulations (data not shown). For this approximation, the hydrodynamic diffusion tensor is $\boldsymbol{H}_{ij} = \delta_{ij}\boldsymbol{I}k_B T/\zeta$, where δ_{ij} is the Kronecker delta and ζ is drag coefficient on a bead.

The springs in the chain have a spring force given by the Finitely Extensible Nonlinear Elastic (FENE) force relation [23]

$$F = \frac{HQ}{1 - (Q/Q_0)^2}, \tag{26}$$

where Q is the extension of the spring, Q_0 is the maximum spring extension, and $H = 3k_B T/(A_k Q_0)$. This relation, which is an approximation of the response of a FJC, is used to be consistent with the model of electrophoretic mobility which used a FJC. All chains in this article are chosen to approximately represent λ-DNA, which has approximately 160 Kuhn steps in the whole chain when dyed [24]. The beads also interact with an exclude volume potential which represents the preference of the polymer coils represented by the springs to not be overlapping. This potential between beads i and j is a soft Gaussian given by [21]

$$U_{ij} = \frac{1}{2}\upsilon k_B T N_{k,s}^2 \left(\frac{3}{4\pi S_s^2}\right)^{3/2} \exp\left(\frac{-3r_{ij}^2}{4S_s^2}\right), \tag{27}$$

where υ is the excluded volume parameter, r_{ij} is the distance between the two beads, and $S_s^2 = N_{k,s}A_k^2/6$ is the squared radius of gyration of an ideal chain consisting of $N_{k,s}$ Kuhn segments per spring.

III. RESULTS AND DISCUSSION

A. Straight channel migration

One important observation in both experiments and simulations that results from conformation-dependent electrophoretic

mobility is the migration of polyelectrolytes across streamlines in straight channels with both pressure-driven flow and electric fields applied in a parallel manner [1,9,10]. Therefore, this acts as an important validation of our new coarse-grained model. The results of Ref. [9] describe a mechanism for the migration. Specifically, the pressure-driven flow will deform the polymer from its coiled and isotropic state. This change in conformation changes the mobility. In particular, the major axis of the radius of gyration tensor is tilted at an angle relative to the electric field which leads to a migration velocity across the channel. Our coarse-grained model can also migrate but in which the reason for the change in mobility and the way it is captured in the model are different. In the model of Ref. [9], the beads which can be relatively far apart along the polymer contour directly interact with EHIs. Instead, our model only includes the interactions within a single rod of each Kuhn segment, which gives a spring a mobility that depends on its extension and orientation.

In the simulations, a parabolic fluid velocity profile $\boldsymbol{u}^\infty$ is imposed along with a constant electric field $\boldsymbol{E}$. The fluid flow is in the x direction and is given by $u_x^\infty = \overline{\gamma}H(1 - (y/H)^2)$, where $\overline{\gamma}$ is the average shear rate, y is the distance from the center of the channel, and H is the half height of the channel. The strength of the fluid flow is quantified by a Weissenberg number as $Wi = \overline{\gamma}\tau$ where τ is the longest Rouse relaxation time given by $\tau = \zeta/\{8H\sin^2[\pi/(2N_b)]\}$. The electric field points parallel to the x-direction, is uniform across the channel, and with strength quantified by an electric Weissenberg number Wi^E. Because the electric field is uniform, this is not defined using a gradient of the electric field. Instead, it is defined such that $Wi^E = Wi$ corresponds to the condition when $\mu_0 E$ equals the mean fluid flow. With this definition, $Wi^E = 3\mu_0 E\tau/(2H)$. The experiments and simulations in Ref. [1,9] correspond to $Wi = 0.9$ and $Wi^E = \pm 1.9254$.

We have simulated dumbbell, five-bead chain, and ten-bead chain using our new model in the straight channels. In addition to simulating with our new coarse-grained mobility model, we also performed simulations with a five-bead chain including explicit EHI between beads as in the model in Ref. [9] to verify the new model. The simulation data represents an average of 50 trajectories, with initial conformations for each obtained from long-time equilibrium runs. Each trajectory is simulated for 20 wall diffusion times [where the wall diffusion time is $N_b\zeta H^2/(k_B T)$], which is sufficient to obtain accurate steady-state profiles.

Figure 1 shows the normalized probability distributions across the channel of the polymer center of mass for cocurrent and countercurrent conditions. Similar to experiments and previous simulations, we find migration to the channel center in cocurrent operation and migration to the channel walls in countercurrent operation. The distributions for our model with different numbers of beads are qualitatively similar and appear to be approaching a limiting profile for large numbers of beads. This is typical when examining a series of coarse-grained models with different numbers of beads. In a dumbbell model the drag is only exerted on two beads instead of along the entire contour. The figure also compares our new model with a five-bead chain that uses explicit EHI between beads instead of a mobility of a spring that varies with stretch of the spring. In
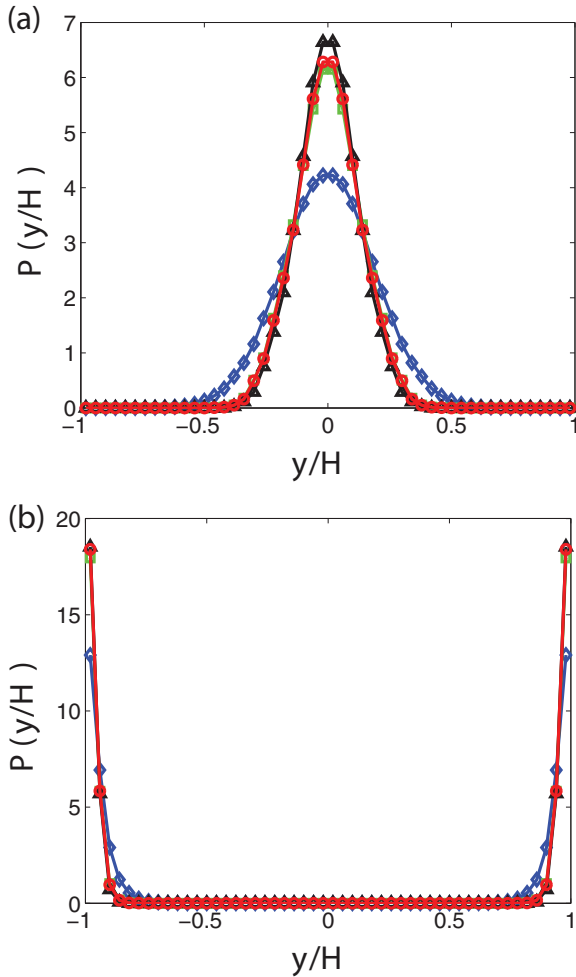
FIG. 1. (Color online) (a) Distribution of polymers across the channel in cocurrent operation with $Wi = 0.9$ and $Wi^E = 1.9254$. The results with a five-bead chain using explicit EHI are shown with red circles. The results with our new model are shown for chains with two beads (blue diamonds), with five beads (green squares), and with ten beads (black triangles). (b) Distribution of polymers across the channel in countercurrent operation with $Wi = 0.9$ and $Wi^E = -1.9254$. The results with a five-bead chain using explicit EHI are shown with red circles. The results with our new model are shown for chains with two beads (blue diamonds), with five beads (green squares), and with ten beads (black triangles).

both cocurrent and countercurrent cases, the two approaches are almost quantitatively the same.

The results in this section validate the new model in situations in which the polymer is weakly deformed from equilibrium and show that the model can capture migration perpendicular to the electric field. However, one of the main advantages of the new model is that it can easily capture the response when the molecule is highly stretched, such as in extensional electric field gradients, which are examined in the next section.

B. Stretching in an electric field gradient

Electric field gradients have been used extensively to stretch DNA in microfluidic devices. In electrostatics, the electric field
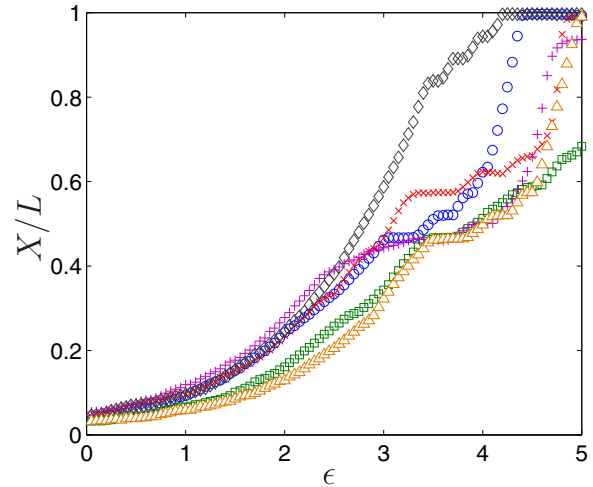

FIG. 2. (Color online) The visual stretch X relative to the contour length L as a function of Hencky strain ϵ (dimensionless time) for $Wi^E = 90$. The different symbols represent different molecules.

has zero curl, which can facilitate large stretching of the DNA. Experimentally, it has been observed that DNA molecules have different mobilities when stretched. When a molecule is stretched in a strong extensional field, a number of folded and kinked configurations are observed [25,26]. The work of Ref. [11] showed that these folds and kinks can lead to configurations that have the same visual length but a different mobility. They developed a one-dimensional (1D) model that explained this phenomena by writing the mobility in terms of the average alignment of a Kuhn segment. In this section, we show simulations of our 3D model in extensional field gradients. The dynamics of the molecules will lead to a variety of configurations including kinks and folds.

In the simulations we impose a planar extensional field given by $E_x = \dot{\epsilon}^E x$, $E_y = -\dot{\epsilon}^E y$, $E_z = 0$ without an external fluid flow. The electric field gradients are quantified by a Weissenberg number Wi^E defined by $Wi^E = \mu_0 \dot{\epsilon}^E \tau$, which uses the nominal mobility μ_0. Note that this definition is different from the one used in the straight channels in the previous section. Simulations are performed using a polymer model made of 20 beads (19 springs) so that kinked and folded configurations can be observed. The starting configurations are taken from an equilibrium distribution, which are obtained by running long-time no-field simulations. For each value of Wi^E, 50 trajectories are simulated with independent starting configurations.

From the equilibrium starting configurations, the extensional field is imposed for a total of five Hencky strain units. The Hencky strain is defined as $\epsilon = \mu_0 \dot{\epsilon}^E t$. Figure 2 shows the stretch of individual molecules versus Hencky strain with $Wi^E = 90$. The stretch is defined in terms of the "visual length," i.e., the maximum x position of a bead minus the minimum x position of a bead. For this relatively large value of Wi^E, the molecules can stretch to a significant fraction of their contour length. The details of stretching are different for each molecule primarily due to their different starting configurations, which is known as "molecular individualism" [26,27].
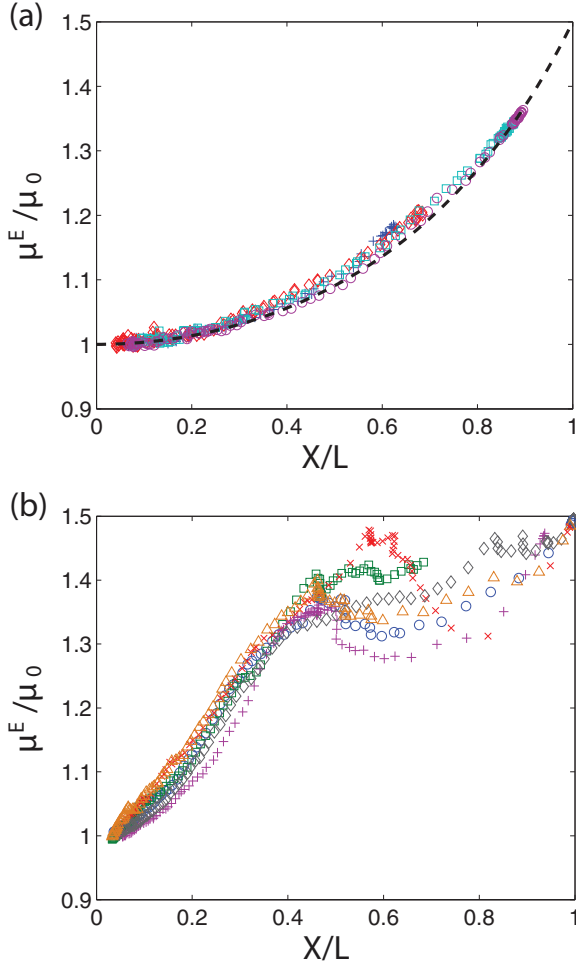
(a)

(b)

FIG. 3. (Color online) (a) The mobility μ^E relative to μ_0 as a function of the visual stretch relative to the contour length for $Wi^E = 3$. The different symbols represent different molecules. The dashed line is $1 + (X/L)^2/[3 - (X/L)^2]$, which is the parallel mobility of a spring. (b) The mobility μ^E relative to μ_0 as a function of the visual stretch relative to the contour length for $Wi^E = 90$. The different symbols represent different molecules.

As the molecules stretch, the mobility changes. The mobility of a molecule is calculated from the speed of the center of mass for a time step (from the change in position divided by the time step) and dividing by the magnitude of the electric field at the position of the center of mass. For the relatively large Wi^E examined here, the Brownian contribution to the motion of the center of mass is small compared to the deterministic contribution. In general, the mobility is a tensor, and the velocity vector and electric field vector are not parallel. However, the "compressional axis" of the field naturally pushes the molecule to the axis where the velocity and electric field are approximately parallel.

Figure 3 shows the mobility of molecules as a function of their visual stretch for $Wi^E = 3$ and $Wi^E = 90$. The value $Wi^E = 3$ is large enough to stretch the molecules but small enough that kinked and folded configurations are not common. The value $Wi^E = 90$ is large enough to produce many kinked and folded configurations. Similar to experiments [11], the molecules show an increasing mobility relative to μ_0 as
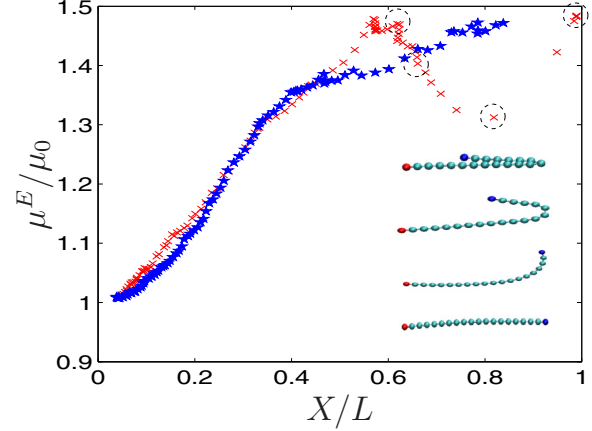

FIG. 4. (Color online) The mobility μ^E relative to μ_0 as a function of the visual stretch relative to the contour length for $Wi^E = 90$. The red $\times$ symbols are the same from Fig. 3 and use the full model. The blue stars use a conformation-dependent mobility that is the same for all beads. The images show the conformations of the full model at the points with circles, with the smallest stretch at the top and the largest stretch at the bottom.

the stretch increases. For the lower Wi^E, all molecules lie essentially on a single curve. Because there are no significant kinks or folds, the molecules all stretch qualitatively the same. For comparison, the function $1 + (X/L)^2/[3 - (X/L)^2]$ is shown, which represents how the mobility parallel to the field changes with the fractional extension of a spring [see Eq. (21) with $\mu_1 = \mu_0/4$].

When a molecule forms a folded or kinked configuration, the polymer backbone is stretched and aligned with the field, leading to an increase in mobility while the overall stretch is not near its maximum value. This is shown in Fig. 3(a) with $Wi^E = 90$. For many trajectories, the mobility increases to a large value when the stretch is approximately half of the contour length. As the stretch increases further, the mobility remains approximately constant. This corresponds to a molecule that unfolds while remaining stretched and aligned with the field. However, some molecules show a significantly drop and then increase in mobility while it unfolds to near full extension.

Figure 4 shows an example of one of these trajectories showing snapshots of the molecule configuration as it unfolds. The width of the molecule increases and part of the molecule points along the compressional axis. This is surprising since one might expect the compressional field to keep the molecule "thin" in that direction while it is stretching, and we are not aware of single molecule visualization experiments that show this type of unraveling. We have determined the mechanism for this unraveling, which is due to the conformation-dependent mobility of the chain when the molecule is in a region with a large value of the electric field (far from the origin).

For the bead-spring chain used here, there is no external fluid flow and explicit hydrodynamic or EHIs have not been included. For these conditions and for the linear electric field with $\boldsymbol{E} = \boldsymbol{\kappa} \cdot \boldsymbol{r}$, Eq. (23) for the dynamics of a bead becomes

$$d\boldsymbol{r}_i = \left[\boldsymbol{\mu}_i \cdot \boldsymbol{\kappa} \cdot \boldsymbol{r}_i + \frac{1}{\zeta} \boldsymbol{F}_i \right] dt + \sqrt{\frac{2k_B T \, dt}{\zeta}} d\boldsymbol{W}_i, \quad (28)$$

where $\boldsymbol{\mu}_i$ is the mobility of bead i. By taking the difference between the equations for $i+1$ and i, we can obtain an update equation for the vector connecting two beads $\boldsymbol{Q}_i = \boldsymbol{r}_{i+1} - \boldsymbol{r}_i$. In particular, we obtain

$$d\boldsymbol{Q}_i = \left[\boldsymbol{\mu}_{i+1} \cdot \boldsymbol{\kappa} \cdot \boldsymbol{Q}_i - (\boldsymbol{\mu}_i - \boldsymbol{\mu}_{i+1}) \cdot \boldsymbol{\kappa} \cdot \boldsymbol{r}_i + \frac{1}{\zeta} (\boldsymbol{F}_{i+1} - \boldsymbol{F}_i) \right] dt$$
$$+ \sqrt{\frac{2k_B T \, dt}{\zeta}} (d\boldsymbol{W}_{i+1} - d\boldsymbol{W}_i). \qquad (29)$$

The spring forces and excluded volume forces on each bead only depend on differences between positions and hence only depend on the spring vectors. However, in general, the electric field terms do depend on the absolute position of the chain because of the explicit $\boldsymbol{r}_i$ even though the gradient of the electric field is a constant (i.e., it is a "homogeneous" field). This is because the values of $\boldsymbol{\mu}_i$ and $\boldsymbol{\mu}_{i+1}$ are not the same. In our model, we choose the mobility of a bead to be the average of the mobilities of the springs connected to the bead. Therefore, unless a dumbbell is used (a single spring), the mobilities of neighboring beads are not equal and the dynamics of a spring depends on the absolute position of the chain relative to the stagnation point. It is this term which leads to the uncommon unraveling.

In order to test this idea, we have also simulated a new type of model. In this model, each spring still has a varying mobility as a function of extension of the spring. However, we calculate the average of these spring mobilities and assign that one average value to all beads. Figure 4 shows the mobility versus stretch for two molecules, both with the same initial condition, but with different choices for the mobility. One molecule is the same from Fig. 3(b) in which the mobility of a spring is the average of the mobilities of the springs connected to it. The other molecule assigns the same mobility to each bead as the average of the spring mobilities. This second molecule also produces a kinked configuration leading to a rising mobility up to a stretch of approximately 0.5. However, the unraveling proceeds in a different way; this second molecule retains a high mobility as the stretch increases because it remains thin in the compressional direction. This comparison shows that the

unique dynamics and stretching can occur when the mobility depends on conformation and when different parts of the same molecule have different mobilities.

IV. CONCLUSION

Polyelectrolytes that are deformed in fluid flows and electric fields change their electrophoretic mobility depending on their conformation. This change is due to EHIs between parts of the polymer. There are some similarities but key differences with how HIs lead to conformation-dependent drag. The changes in mobility occur for even relatively short polymers, and are approximately a local effect along the polymer backbone when its is strongly stretched from equilibrium. In this article, we have developed a new coarse-grained model that can be used for dynamical simulations of polymers like ds-DNA in combinations of fluid flows and electric fields. The model assigns an electrophoretic mobility tensor to each bead that is a function of the stretch and orientation of the springs that are connected to the bead. The model has been validated in two situations: combined electrophoresis and pressure-driven flow in a channel with the polymer weakly deformed from equilibrium and planar extensional electric field gradients that stretch the polymer far from equilibrium. In capillary electrophoresis the model captures the cross-stream migration due to stretching of the chain at an angle to the electric field. In strong extensional fields the model captures the folded and kinked configurations that have a large impact on the mobility of the chain. For large electric fields, the model shows the chain can unravel these folds in a way not seen previously in simulations or experiments. The unique unfolding is due to the fact that the dynamics are dependent on the location of the center of mass of the chain even though the electric field gradients are uniform in the system. This coarse-grained model will allow for rapid simulations in situations with combinations of electric fields and fluid flows, for example in the trapping and manipulation of molecules in microfluidic devices, which will be shown in a subsequent article.

[1] J. Zheng and E. S. Yeung, Anal. Chem. **74**, 4536 (2002).

[2] J. Zheng and E. S. Yeung, Anal. Chem. **75**, 3675 (2003).

[3] J. Zheng and E. S. Yeung, Aust. J. Chem. **56**, 149 (2003).

[4] J. Zheng, H.-W. Li, and E. S. Yeung, J. Phys. Chem. B **108**, 10357 (2004).

[5] D. Long and A. Ajdari, Eur. Phys. J. E **4**, 29 (2001).

[6] J. E. Butler, O. B. Usta, R. Kekre, and A. J. C. Ladd, Phys. Fluids **19**, 113101 (2007).

[7] O. B. Usta, J. E. Butler, and A. J. C. Ladd, Phys. Rev. Lett. **98**, 098301 (2007).

[8] R. Kekre, J. E. Butler, and A. J. C. Ladd, Phys. Rev. E **82**, 011802 (2010).

[9] R. Kekre, J. E. Butler, and A. J. C. Ladd, Phys. Rev. E **82**, 050803(R) (2010).

[10] M. Arca, J. E. Butler, and A. J. C. Ladd, Soft Matter **11**, 4375 (2015).

[11] W.-C. Liao, N. Watari, S. Wang, X. Hu, R. G. Larson, and L. J. Lee, Electrophoresis **31**, 2813 (2010).

[12] R. G. Larson, J. Rheol. **49**, 1 (2005).

[13] A. Balducci, P. Mao, J. Han, and P. S. Doyle, Macromolecules **39**, 6273 (2006).

[14] C. M. Schroeder, E. S. Shaqfeh, and S. Chu, Macromolecules **37**, 9242 (2004).

[15] J. Tang, D. W. Trahan, and P. S. Doyle, Macromolecules **43**, 3081 (2010).

[16] R. Radhakrishnan and P. T. Underhill, Macromolecules **46**, 548 (2013).

[17] A. Cohen, Rheol. Acta **30**, 270 (1991).

[18] D. L. Ermak and J. A. McCammon, J. Chem. Phys. **69**, 1352 (1978).

[19] P. S. Grassia, E. J. Hinch, and L. C. Nitsche, J. Fluid Mech. **282**, 373 (1995).

[20] J. S. Hur, E. S. Shaqfeh, and R. G. Larson, J. Rheol. **44**, 713 (2000).

[21] R. M. Jendrejack, J. J. de Pablo, and M. D. Graham, J. Chem. Phys. **116**, 7752 (2002).

[22] C.-C. Hsieh, L. Li, and R. G. Larson, J. Non-Newtonian Fluid Mech. **113**, 147 (2003).

[23] H. R. Warner, Jr., Ind. Eng. Chem. Fundam. **11**, 379 (1972).

[24] E. S. Shaqfeh, J. Non-Newtonian Fluid Mech. **130**, 1 (2005).

[25] T. T. Perkins, D. E. Smith, and S. Chu, Science **276**, 2016 (1997).

[26] R. G. Larson, H. Hu, D. E. Smith, and S. Chu, J. Rheol. **43**, 267 (1999).

[27] P. G. de Gennes, Science **276**, 1999 (1997).